

PAPER • OPEN ACCESS

Formation of regularly spaced networks as a general feature of actin bundle condensation by entropic forces

To cite this article: Florian Huber *et al* 2015 *New J. Phys.* **17** 043029

View the [article online](#) for updates and enhancements.

You may also like

- [Self-organized nanocrack networks: a pathway to enlarge catalytic surface area in sputtered ceramic thin films, showcased for photocatalytic TiO₂](#)
B Henkel, A Vahl, O Ç Aktas *et al.*
- [Triadic closure dynamics drives scaling laws in social multiplex networks](#)
Peter Klimek and Stefan Thurner
- [Complex Networks: from Biology to Information Technology](#)
A Barrat, S Boccaletti, G Caldarelli *et al.*

Recent citations

- [Tuning the Properties of Active Microtubule Networks by Depletion Forces](#)
Vahid Nasirimarekani *et al*
- [Cells in Slow Motion: Apparent Undercooling Increases Glassy Behavior at Physiological Temperatures](#)
Jörg Schnauß *et al*
- [Regulation of Actin Bundle Mechanics and Structure by Intracellular Environmental Factors](#)
Nicholas Castaneda *et al*



PAPER

OPEN ACCESS

RECEIVED
22 October 2014REVISED
3 March 2015ACCEPTED FOR PUBLICATION
4 March 2015PUBLISHED
15 April 2015

Content from this work
may be used under the
terms of the [Creative
Commons Attribution 3.0
licence](#).

Any further distribution of
this work must maintain
attribution to the
author(s) and the title of
the work, journal citation
and DOI.



Formation of regularly spaced networks as a general feature of actin bundle condensation by entropic forces

Florian Huber^{1,2}, Dan Strehle^{1,3}, Jörg Schnauß¹ and Josef Käs¹¹ Institute for Experimental Physics I, University of Leipzig, Leipzig, Germany² FOM Institute AMOLF, Amsterdam, The Netherlands³ Laboratoire Photonique, Numérique et Nanosciences, Institut d'Optique, Bordeaux, FranceE-mail: f.huber@amolf.nl and jkaes@physik.uni-leipzig.de**Keywords:** actin network formation, molecular crowding, counterion condensation, entropic forces, network formation kinetics

Abstract

Biopolymer networks contribute mechanical integrity as well as functional organization to living cells. One of their major constituents, the protein actin, is present in a large variety of different network architectures, ranging from extensive networks to densely packed bundles. The shape of the network is directly linked to its mechanical properties and essential physiological functions. However, a profound understanding of architecture-determining mechanisms and their physical constraints remains elusive. We use experimental bottom-up systems to study the formation of confined actin networks by entropic forces. Experiments based on molecular crowding as well as counterion condensation reveal a generic tendency of homogeneous filament solutions to aggregate into regular actin bundle networks connected by aster-like centers. The network architecture is found to critically rely on network formation history. Starting from identical biochemical compositions, we observe drastic changes in network architecture as a consequence of initially biased filament orientation or mixing-induced perturbations. Our experiments suggest that the tendency to form regularly spaced bundle networks is a rather general feature of isotropic, homogeneous filament solutions subject to uniform attractive interactions. Due to the fundamental nature of the considered interactions, we expect that the investigated type of network formation further implies severe physical constraints for cytoskeleton self-organization on the more complex level of living cells.

Introduction

The cytoskeleton, a self-organizing biopolymer network, is essential for the spatial and functional organization of living cells. The protein actin is a central cytoskeleton building block able to form dynamic yet stable semiflexible filaments. Actin filaments (F-actin) form the basis of numerous different network architectures ranging from extensive interwoven networks, as found at the leading edge of migrating cells (lamellipodium,) to densely packed bundles of filaments in stress fibers and filopodia [1, 2].

The network architecture is known to dramatically affect the macroscopic mechanical properties [3–6]. Further, many actin-related proteins bind in a structure-specific manner thereby translating different network architectures into different cytoskeletal functions [7]. It remains little understood, however, how different cytoskeletal architectures are triggered and spatially restricted or controlled. A central question is how the different cytoskeletal structures can be formed and maintained in parallel while sharing a pool of identical ingredients. For a long time, a great deal of attention was paid to various cross-linking proteins. They differ in size, shape, and binding affinity and in some cases indeed tend to induce particular network architectures such as branched networks formed with Arp2/3 [8]. More recently, it has become increasingly clear that the type of cross-linker is only one among many architecture-defining parameters.

Reconstituted model systems revealed that spatial control over filament nucleation has a major influence on resulting network shapes [9]. Even in the absence of nucleation patterns, however, several experimental [6, 10]

as well as theoretical studies [11, 12] revealed that a particular actin network architecture cannot be properly attributed to individual types of protein cross-linkers. For conventional protein cross-linkers, the F-actin density, as well as the relative amount of cross-linkers, were found to be key parameters determining network architecture [3, 6, 11]. Networks formed at very low cross-linker densities tend to be more filament dominated, while extensive bundle networks have been reported at high cross-linker densities [3, 6]. With the exception of cross-linkers entirely unable to bind to parallel filaments, all linker-filament systems can lower their free energy by forming parallel bundles at very high linker densities [11]. This is mainly due to the increased number of potential linker binding sites offered by a parallel bundle geometry. Even for linkers that can be considered pure bundling agents, splaying and merging of bundle segments still culminates in bundle networks at high enough filament densities [6, 13]. Interestingly, recent observations further show that assembly kinetics directly impact the final appearance of keratin [14] as well as actin networks [15, 16].

These examples clearly show that spatial and temporal control of filament nucleation, filament growth dynamics, and cross-linking is necessary to obtain one particular network architecture. In addition, physical constraints from the proteins' environment will drastically affect their interactions. Geometrical confinement has been reported to have a significant influence on filament orientations [17, 18] and network geometries [19, 20]. Additionally, bundle formation has been observed to be induced by membrane tension [21]. Other key factors that we expect to play a major role during network formation include ionic conditions, excluded volume effects, and viscosity.

It is well known that polyelectrolyte effects like counterion condensation, as well as excluded volume effects creating depletion forces, are able to induce filament aggregation [22, 23]. In this article we will focus on these mechanisms for three main reasons. First, they allow neglecting the particularities of the conventional cross-linker's molecular structure. Second, their role in restricting and determining cytoskeleton architecture has not yet received much attention, although a physiological relevance is likely. Cells show a macromolecule content of up to 40% [24], making crowding effects very plausible. In addition, many multivalent ions can have severe effects already at comparably low concentrations, and different types of multivalent ions can function in an additive manner [22]. Third, we make use of the fact that—unlike protein cross-linkers—both crowding agents and counterions only start to aggregate actin filaments after reaching a critical concentration [22, 23]. This enables us to effectively apply them as a switchable cross-linker [20, 25]. Therefore, we are able to separate mixing effects from aggregation effects. Our experiments reveal that aggregation-induced network architectures critically depend on the formation history and the presence of anisotropies.

Results

Controlled formation of actin bundle networks using crowding agents or counterions

Some of the most commonly applied polymers to mimic molecular crowding *in vitro* are PEG (polyethylene glycol), dextran (a polysaccharide), and methylcellulose. In addition, the protein albumin is often used for similar purposes and to inhibit unspecific binding and adsorption. Although the excluded volume effect should in the first approximation only depend on size and density of the applied crowding agents, the different physical and the very different chemical properties of the crowding agents might lead to substantial differences on the microscopic scale [26]. In the present study we mainly focused on PEG as a highly soluble and non-interacting polymer and BSA (bovine serum albumin) representing a protein found in living systems supposed to have no specific interactions with actin. We further tested dextran, which is very commonly applied as a crowding agent, as well as methylcellulose, representing a comparably hydrophobic crowding agent commonly used for its strong influence on viscosity [27, 28].

Both crowding agents and counterions induce filament aggregation as soon as their concentration exceeds a critical threshold [22, 23, 25]. The threshold value itself can be shifted by the addition of monovalent ions [22, 23]. We applied two complementary techniques to gently move our experimental system from nonaggregating conditions ($<$ critical threshold) into the aggregating regime ($>$ critical threshold). Thereby, we aimed at observing network formation in a nearly unperturbed system upon fast and homogeneous initiation of aggregation. In the first method, droplets deposited on a passivated glass surface were subject to slow, controlled evaporation. This reduced the water content and thereby raised the ion or crowding agent concentration (figures 1(A)–(B)). In the second method, two thin-flow chambers were separated by a dense hydrogel, allowing ion diffusion but no actin filament exchange (figures 1(C)–(D)).

With both methods, *in situ* polymerized actin filament solutions were exposed to aggregating conditions without macroscopic disturbances from mixing. As soon as crowding agents or counterions exceeded the threshold concentration, a rapid transition from a homogeneous F-actin solution to bundled actin networks is observed (figure 2).

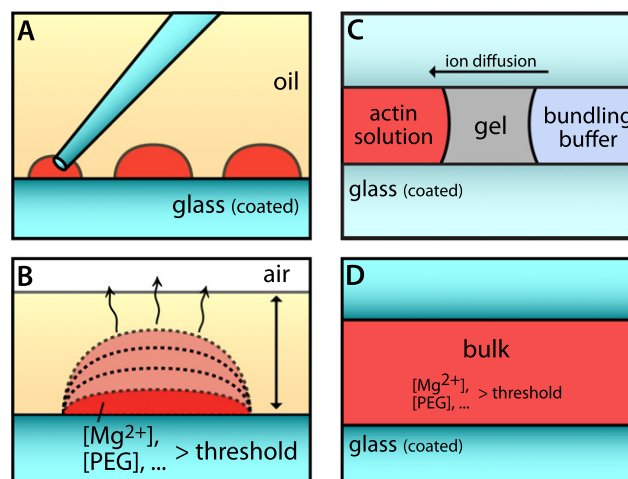


Figure 1. Different experimental procedures were applied to aggregate actin filaments. Small droplets (20–200 μm diameter) are deposited on a glass surface protected by an oil layer (A). Through reduction of the oil, layer-thickness evaporation is controlled to slowly increase the salt and crowding agent concentration within the droplets until reaching a critical aggregating threshold (B). Diffusion chambers consist of two neighboring flow channels separated by a porous agarose gel. Increasing ion concentrations through diffusion across the agarose barrier shift the actin filament solution towards the aggregation transition (C). Finally, networks were also formed by gently mixing more concentrated salt/crowding agent solutions with F-actin solutions, which were then confined between two glass plates (D).

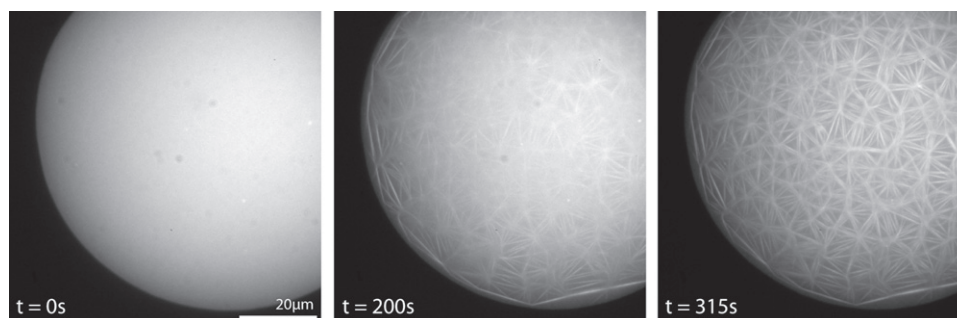


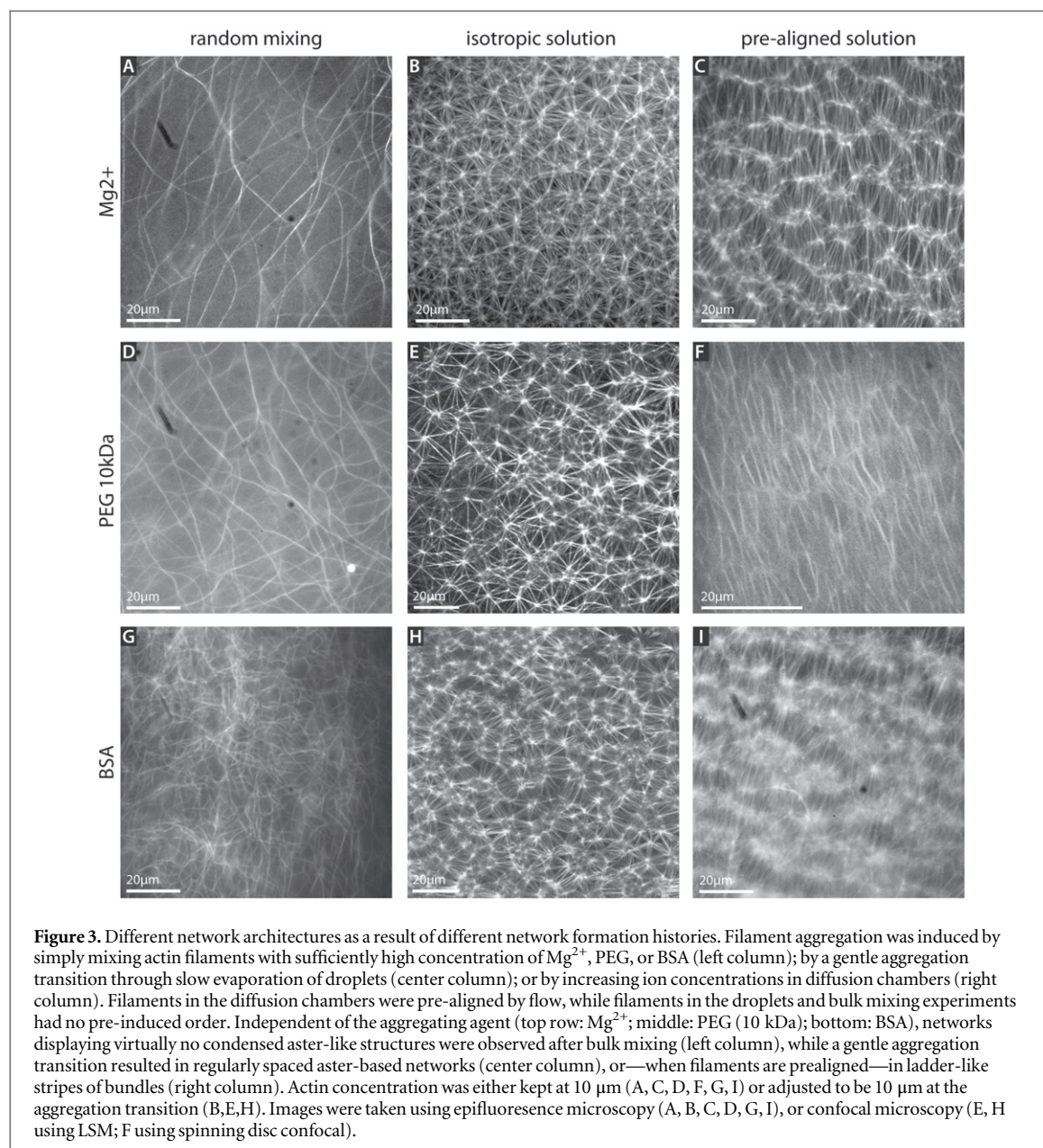
Figure 2. Actin network formation after reaching the critical concentration of Mg^{2+} ions (onset at $t = 0\text{ s}$). Driven by counterion condensation, a regularly spaced actin bundle network forms throughout the entire droplet within around 5 minutes. Images were taken using epifluorescence microscopy.

Comparison of different network formation processes

A common way to form actin networks *in vitro* is to mix preformed actin filaments with a solution containing protein cross-linkers or to initiate rapid polymerization of actin in the presence of cross-linkers by adding a concentrated F-buffer. When actin filaments were mixed by gentle pipetting with a solution of high Mg^{2+} or crowding agent concentrations, random actin bundle networks formed (figure 3, left column). Mixing was gentle enough to create networks that displayed a homogeneous actin bundle density. However, these networks displayed virtually no condensed aster-like centers. Regarding bundle orientation or average free bundle lengths, we could not find any sign of higher order, and resulting networks strongly resembled cross-linked actin networks, as depicted elsewhere [6, 29, 30].

Using slowly evaporating droplets or diffusion chambers (figure 1), it was possible to temporally separate mixing effects from aggregating effects. Hence, the system could equilibrate after mixing before the onset of filament aggregation. Actin bundle networks obtained in the absence of mixing effects showed entirely different network architectures, although the biochemical conditions chosen were identical (same actin and ion concentrations).

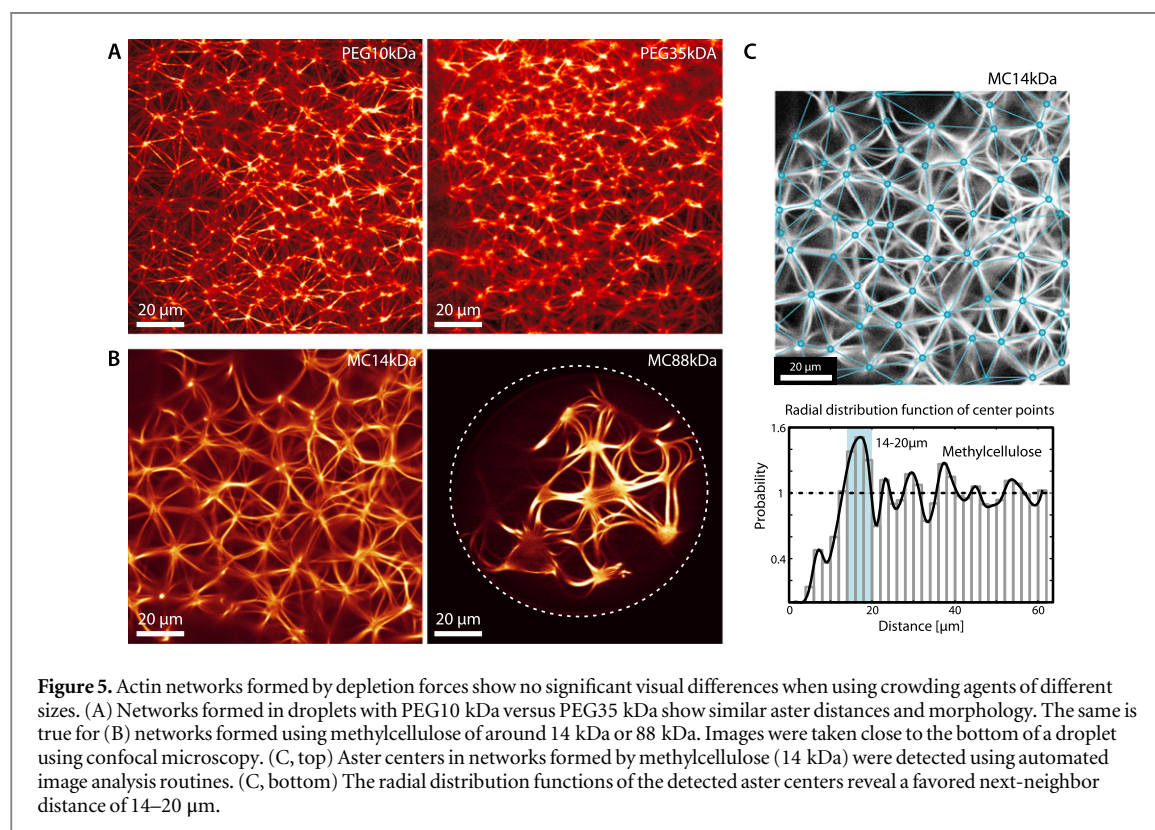
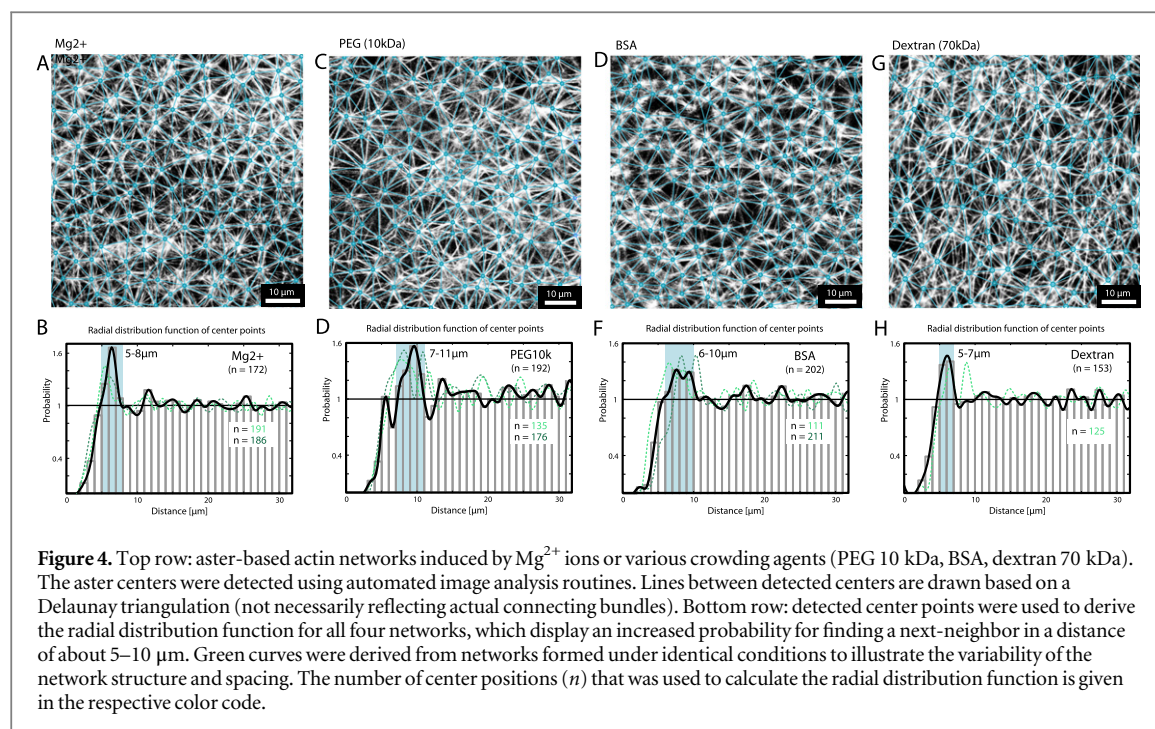
For moderate actin concentrations ($<40\text{ }\mu\text{M}$ at the aggregation transition, [25]), we observed a very robust formation of regularly spaced aster-based bundle networks (figures 2, 3, center column). Deposition of droplets did not include a dominant single-flow axis that would have been able to globally align actin filaments. To further remove potentially remaining anisotropies in local filament order, droplets were incubated for one hour prior to the onset of controlled evaporation through partial oil removal (see ‘Materials and Methods’ section). It is important to note at this point that evaporation was still progressing slowly, so that the droplet volume



changed by only 5% to 10% between the first visible signs of aggregation and the fully developed bundle networks [25].

To our surprise, we found the formation of a similar aster-based network architecture to be a very robust, general feature for entropic aggregation mechanisms as long as the initial filament order was isotropic and as long as the aggregation transition was induced gently to not cause notable material flow. Closely resembling aster-based networks could be obtained for entirely different entropic aggregation mechanisms ranging from counterion condensation (Mg^{2+}) to molecular crowding through inert polymers (PEG) or globular proteins (BSA) (figure 3). In addition to PEG and BSA, we observed the formation of aster-based networks for crowding-induced bundling through polysaccharides (dextran, 70 kDa, figure 4(D)) or methylcellulose (figure 5(B)). To see if the size of the crowding agent in solution (roughly its radius of gyration [23]) has an influence on the final network architecture, we further tested PEGs and methylcelluloses of different molecular weights (figure 5). Upon changes in the crowding agent size, we only noted a changed critical concentration necessary to induce filament aggregation. However, the respective actin networks for each of the crowding agents showed no dependence on the crowding agent size. We also observed no qualitative changes in network architecture or average aster distance when changing the droplet diameter (figure 6), underlining that the preferred aster spacing is largely independent of the spatial confinement.

For all crowding agents used we were able to observe aster-based networks. Interestingly, aster center positions were correlated, showing signs of regularity in the form of preferred aster-to-aster distances on the order of 5–10 μm (figure 4). While methylcellulose-induced bundle networks form qualitatively resembling



aster-based networks, we also noted few quantitatively differing characteristics compared to all other networks tested. At a comparable actin concentration (15–20 μm when reaching the bundling threshold), bundle diameters appeared substantially larger (figure 5(B)), and the preferred aster-to-aster distance was roughly twice as long as for the other networks (14–20 μm, figure 5(C)). We speculate that the observed differences might be due to the comparably high hydrophobicity of methylcellulose itself and the strong interactions between individual molecules, which ultimately causes the formation of methylcellulose gels at high temperatures [27]. Another major difference between the various crowding agents is the threshold concentration at which they induce actin network formation. Considerable densities of PEG (10 kDa) or BSA were necessary to induce

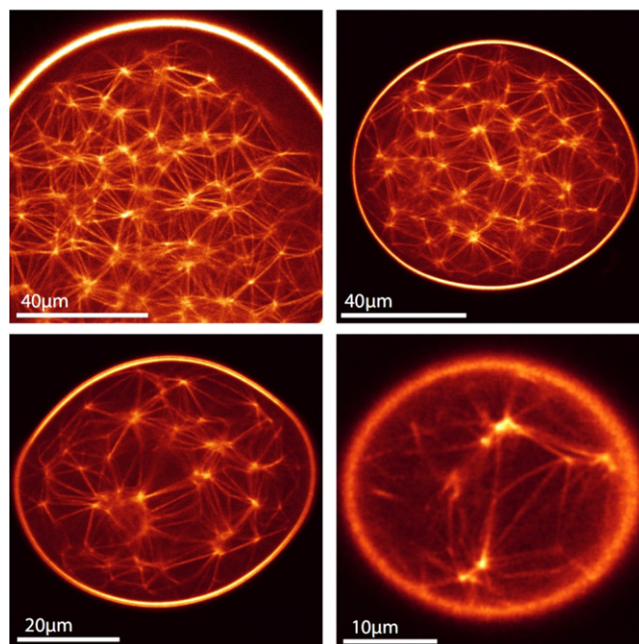


Figure 6. Actin bundle networks were formed using Mg^{2+} counterions in droplets of different sizes. For droplet diameters larger than around $10\text{ }\mu\text{m}$, we observed aster formation. Patterns appeared to be largely independent of droplet size with virtually unchanged aster distances. Images were taken close to the bottom of a droplet using confocal microscopy.

bundling (we measured $60 \pm 10 \frac{\text{mg}}{\text{ml}}$ for both agents when used at 50 mM KCl). In contrast, much lower concentrations of methylcellulose were sufficient to induce actin filament aggregation ($7 \pm 1 \frac{\text{mg}}{\text{ml}}$ of 14 kDa and $1.2 \pm 0.3 \frac{\text{mg}}{\text{ml}}$ of 88 kDa methylcellulose at 50 mM KCl).

The effect of anisotropies on the final network architecture

Previous work has shown that anisotropies in the form of filament pre-alignment in the initial state of the F-actin solution can drastically influence counterion-induced network formation [25]. However, in those experiments filaments were mainly pre-aligned due to high filament densities. Here we use an improved experimental setup where filaments were pre-aligned by flowing them into thin chambers (figure 1). The initial alignment through flow was memorized by the system for substantial times even at filament concentrations far below the nematic onset [31], assuming long average filament lengths ($10\text{--}20\text{ }\mu\text{m}$).

A 1.5% agarose barrier between two neighboring flow chambers allowed us to gently change buffer conditions without inducing notable flows or turbulences. Due to the relatively large mesh size of around 100 nm [32], ion diffusion should hardly be affected by the agarose gel, but preformed actin filaments were not able to leave the flow channel for the duration of the experiments. To initiate cross-linking by counterions, a buffer solution rich in Mg^{2+} was flushed into the channel next to the one filled with the flow-aligned actin filaments (figure 1(B)). Mg^{2+} diffusion across the agarose barrier then led to a steady increase of counterions in the actin channel, eventually reaching the critical threshold for filament aggregation. When working with depletion forces, preformed actin filaments were mixed with a subthreshold crowding agent concentration at a low monovalent salt level. The addition of concentrated KCl to the buffer channel (figure 1(B)) slowly raised the KCl concentration in the filament channel, which is known to shift the critical concentration of the crowding agent [23], in our case, PEG or BSA.

As the threshold concentration of the respective ion moves across the filament channel, a rapid transition towards actin bundle networks was observed (figure 7). Due to the pre-alignment of filaments through flow, we observe the formation of ladder-like stripes of bundles. Interestingly, the individual stripes display a very homogeneous thickness and were all separated by perpendicular actin bundles (figure 7, bottom row).

Discussion

To date, the formation of aster-based biopolymer networks has mostly been associated with active processes of molecular motors [33–36]. Recently, however, such networks have even been reported for motor-free systems cross-linked by magnesium ions [20, 25]. Here, we report that regularly spaced aster-based networks are a rather

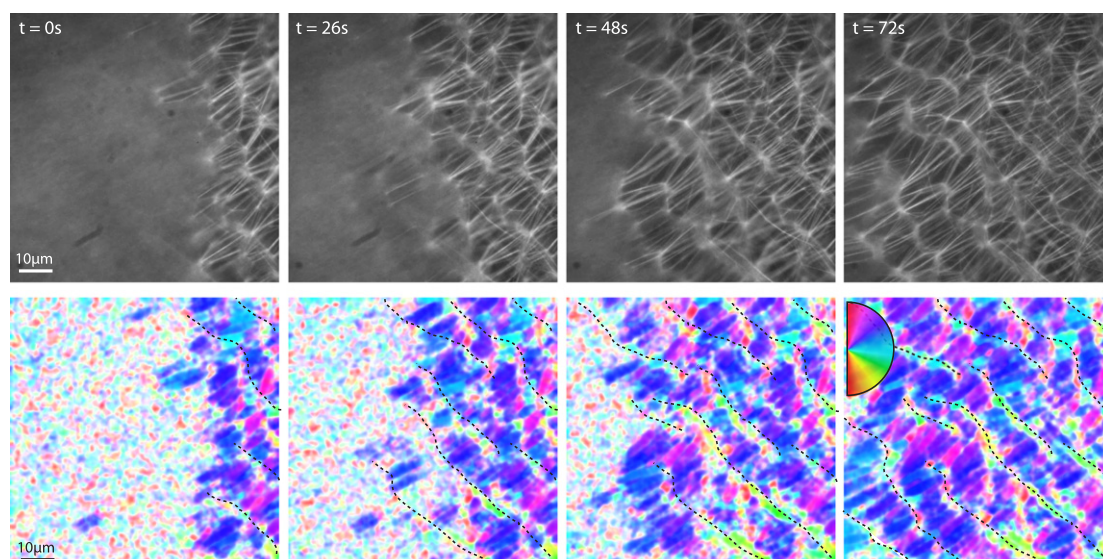


Figure 7. Epifluorescence images show rapid formation of ladder-like stripes of actin bundles as the Mg^{2+} concentration increases across the field of view (top row). A false color representation of the local orientation (see ‘Materials and Methods’ section) reveals the progression of a regular alternating pattern of highly aligned stripes (bottom row). Dashed lines were added to guide the eye along regions that separate neighboring ladder-like stripes of actin bundles.

robust feature that can be obtained by various cross-linking or bundling mechanisms, even in the absence of molecular motor-driven active processes. Counterions, as well as a wide range of crowding agents, are able to drive aster-based network self-assembly. This strongly suggests that the underlying microscopic formation processes are not based on particular ingredients or their according microscopic properties (such as cross-linker geometry). We rather expect the aggregation of filament solutions into regularly spaced aster-based networks to be a general feature of the unspecific, uniform, attractive interactions between filaments in conjunction with a homogeneous, isotropic initial state.

Longitudinal filament transport by molecular motors is not strictly necessary for the formation of aster-like structures. Further, this scenario can explain why the formation of similar aster-based networks has not been reported in earlier studies on the aggregation of F-actin through counterions [37], crowding agents [23, 29], or in studies on protein cross-linkers [6, 30]. *In vitro* experiments commonly face the limitation of having cross-linking effects as soon as the reagents get in contact. As a result, the network formation process is necessarily coupled to either the mixing of cross-linkers and F-actin or the rapid actin polymerization in the presence of cross-linkers. It is clear that in both cases, the network formation process will follow a substantially different history than within our droplet or diffusion chamber experiments. Whenever we applied similar protocols to establish crowding agent or counterion-driven networks in bulk, the resulting networks lacked asters and showed no apparent global regularity (figure 3, left column).

The aster-like networks we present are at first sight visually reminiscent of structures formed in the presence of molecular motors [33–36]. Asters reported for microtubules and motors clearly seem to be energy-dissipating, self-organized structures that rely on motor activity driven by ATP (adenosine triphosphate) [33, 34]. They hence follow very different formation principles. Formerly reported asters in actin networks, however, were either obtained in the presence of rigid cross-linkers [35] or nonactive (ATP-depleted) myosin [36]. Motor activity is able to augment and prolong filament motion. This way, perturbations (or anisotropies) originating from initial convective mixing or rapid polymerization will decay faster. We speculate that in particular the findings described in Smith *et al* [36] could be based on a very similar mechanism than the presented droplet and diffusion chamber experiments since they report a reversible formation of asters upon ATP depletion. This converts myosin motors into nonactive cross-linkers, which effectively corresponds to a motor–cross-linker transition, potentially reflecting an analogue case to the evaporation or diffusion-induced cross-linking in our experiments.

Altogether, the presented findings illustrate that a particular biochemical composition alone is not sufficient to determine the formation of one particular network architecture. In addition to the well-known key parameters filament and linker density, we show that equally strong restrictions on network architecture result from the network formation dynamics and potential perturbations of the solution such as anisotropies in form of a biased filament orientation. In our opinion, this leads to a far more complex picture of cytoskeleton networks *in vivo*. It remains an important task to better understand how local protein concentrations or

nucleation and activation levels of cytoskeleton building blocks are regulated. This, however, will not be sufficient to fully explain the regulation of cytoskeleton architecture. Based on our experimental observations, the time course (or history) of network formation is likely to be crucial as well.

The fact that different formation pathways can lead to very different network morphologies indicates ‘frozen’ metastable states. Those states can still result in extremely stable structures (we observed that our bundle networks remained virtually unchanged for >24 h after stopping evaporation). In living cells, molecular motors and filament turnover additionally add active processes, permanently driving the system out of equilibrium. We speculate that this could further strengthen the time-course sensitivity of cytoskeleton networks. Active processes could, on the other hand, also prevent the system from getting trapped in undesired frozen states.

We further observed very different network architectures for initially isotropic or anisotropic filament solution, which reflects another aspect of a history-dependent formation process. The initial filament order decays slower than the network formation progresses, thereby getting trapped (or ‘frozen’) in the final, very stable bundle network. Anisotropies can be obtained in many ways. We introduced local filament order by moderate flow but high filament densities [25, 38], and boundary effects induced by geometrical confinement [20] have similar effects. Deshpande *et al* [20], for instance, observed bundle networks closely resembling our ladder-like structure when using thin, rectangular microchambers as boundaries.

Hence, anisotropies or perturbations of the isotropic state directly translate into different network architectures. This can yield networks adapting to a rigid [20] or more flexible confinement [19], as well as networks reacting to high filament densities [25] or flow-induced alignment as presented here. Thus, the protein mixture itself represents an autonomous structure sensing (and memorizing) module independent of biochemical regulation [2, 39].

While the simplified nature of our experiments allows exploring rather general physical mechanisms and constraints, further steps will be necessary to translate the presented findings to the level of living cells. Ideally, similar experiments with switchable cross-linkers (e.g., using light-sensitive constructs) might reveal a similar tendency to form regularly spaced aster-based networks when cross-linking is initiated in unperturbed, isotropic systems. Moreover, additional work will also be necessary to better understand why the type of crowding agent influences the network architecture, although the size of the respective crowding agent does not. Those findings demonstrate that the different crowding agents we applied cannot be fully described by first-order excluded volume effects, an issue also raised previously by others [26, 40].

We are certainly not the first to propose that molecular crowding must be considered more carefully for a more complete understanding of cellular processes [24, 26, 40, 41], but our experiments for the first time display the surprisingly rich repertoire of crowding-driven network formation. In the past, reconstituted bottom-up systems proved to be extremely successful when studying cytoskeletal polymer systems and they greatly contributed to our current understanding of cytoskeleton organization [1, 2]. Yet most *in vitro* model systems largely ignored the effects of molecular crowding on cytoskeleton self-organization, although the cell interior can be orders of magnitude more crowded than typical reconstituted model systems. Given the drastic effects that crowding has on reaction rates [26], together with its severe impact of crowding on network formation reported here, we strongly suggest to include molecular crowding more systematically in future experimental model systems to better mimic the physical constraints present in living cells.

Materials and methods

Protein purification

Except for the proteins used, all chemicals were purchased from Sigma-Aldrich (St. Louis, USA). Actin was prepared from rabbit muscle as described previously [38]. The protein was stored in G-buffer (5 mM Tris, 0.1 mM CaCl_2 , 0.2 mM ATP, 1 mM DTT (dithiothreitol), and 0.01% NaN_3). Actin was rhodamine labeled without the use of phalloidin according to [42]. G-actin was mixed with labeled rhodamine actin to a ratio of 10:1 before polymerizing filaments. The final mixture of buffer, salt, actin and crowding agents further contained 25 mM Dabco to suppress photobleaching.

Droplet deposition and diffusion chambers

Droplets were deposited and evaporated as previously described [25]. A glass cover slip was covered by an oil layer (hexadecane) of 250–500 μm height, which practically stopped evaporation. Droplets, 80–120 μm in diameter, were placed on the cover slip surface, and the sample was transferred to a confocal microscope (TCS SP2 AOBs; Leica Microsystems). Subsequently, evaporation was controlled by slightly changing the oil layer’s thickness or by exchanging hexadecane against silicone oil DC200 using a standard micropipette (figures 1(A), (B)). It is important to note that no change in droplet diameter could be observed during the evaporation process. Hence, the volume change only affected the droplet height.

Diffusion chambers (figure 1(C)) were formed by pipetting a small stripe of 1.5% heated agarose solution on a glass cover slip. A glass slide was pressed against the cover slip before cooling of the agarose finally led to gelation of the agarose diffusion barrier. Alternatively, the sample was quickly assembled on a hot plate at 80 °C. Conditions were tuned to facilitate the formation of thin and narrow flow channels on both sides of the agarose stripe (typical volume of 3–4 μl each). Diffusion chambers were visualized using standard epifluorescence microscopy. Glass surfaces in contact with the experimental solutions were initially passivated using Sigmacote (Sigma-Aldrich, St. Louis, USA). After carefully flowing preformed actin filaments (stabilized with phalloidin in a 1:1 ratio) into the actin channel, filament aggregation was initiated by flowing an appropriate high salt buffer into the neighboring channel. For counterion-induced condensation, a buffer of high Mg^{2+} concentration ($>100\text{ mM}$) was used. For aggregation by molecular crowding, 2% (w/v) PEG (10 kDa) or 4% BSA was added to the actin filament buffer. Bundling was then induced by adding a concentrated KCl buffer to the diffusion channel (500 mM KCL).

Bulk bundle networks were formed by carefully mixing polymerized actin with the aggregation-inducing agent (10% PEG 10 kDa, 10% BSA, or 50 mM MgCl_2) with a final actin concentration of 10 μM (figure 1(D)).

Orientation maps

Orientation maps in figure 7 were derived based on fluorescence images using the ImageJ plugin ‘OrientationJ’ employing continuous spatial derivatives to calculate the local orientation and coherency (a measure for the degree of local order) [43]. Images shown were derived by translating the orientation to hue and the coherency to saturation, while the brightness was kept constant. We used 512×512 pixel fluorescence pictures and a Gaussian window of 2 pixels (cubic spline gradient).

Automated center detection and radial distribution function

The experimentally observed aster-based actin networks were further quantified using image analysis routines. To detect aster center positions, an automated software routine was written using MATLAB (the Mathworks, R2013a).

First, network knots were identified using the fact that many bundles point towards these knots. This was done by applying a correlation analysis based on thin lines along different angles (here: 80 steps from 0 to π), together with the Canny algorithm to first enhance more prominent bundles. The lines were elongated further to pronounce the network centers after overlaying the images derived for all directions.

Second, blurring followed by threshold and erosion steps finally allowed us to discriminate the individual centers. When using images of good quality, the developed routine allowed tracing center positions in a very consistent manner. A simple Delaunay triangulation is used to connect the detected center positions to visually illustrate the distances to nearest-neighboring centers (see also [25]). The triangulation-based connections thus do not necessarily reflect actual actin bundles, although we found that most of them do agree well with existing bundle locations.

Using the detected center positions, it was possible to derive the radial distribution function. The average density of centers was set to be the number of found asters divided by the total image area. The expected number of asters to be found at a given distance R for each individual aster was then corrected by the actual fraction of the area RdR that lay within the image boundaries.

Acknowledgments

We would like to thank Klaus Kroy, Anatol Fritsch, and Tobias Kießling for helpful discussions, as well as Matti Gralka for his contributions to an earlier stage of this project. The authors acknowledge funding by the Leipzig School of Natural Sciences ‘BuildMoNa.’ FH was further supported by a Marie Curie IEF fellowship.

References

- [1] Fletcher D A and Mullins R D 2010 Cell mechanics and the cytoskeleton *Nature* **463** 485–92
- [2] Huber F et al 2013 Emergent complexity of the cytoskeleton: from single filaments to tissue *Adv. Phys.* **62** 1–112
- [3] Lieleg O, MMAE C and Bausch A R 2010 Structure and dynamics of cross-linked actin networks *Soft Matter* **6** 218–25
- [4] Wilhelm J and Frey E 2003 Elasticity of stiff polymer networks *Phys. Rev. Lett.* **91** 108103
- [5] Huisman E M, van Dillen T, Onck P R and Van der Giessen E 2007 Three-dimensional cross-linked F-actin networks: relation between network architecture and mechanical behavior *Phys. Rev. Lett.* **99** 208103
- [6] Schmoller K M, Lieleg O and Bausch A R 2009 Structural and viscoelastic properties of actin/filamin networks: cross-linked versus bundled networks *Biophys. J.* **97** 83–9
- [7] Brawley C M and Rock R S 2009 Unconventional myosin traffic in cells reveals a selective actin cytoskeleton *Proc. Natl Acad. Sci. USA* **106** 24

- [8] Svitkina T M and Borisy G G 1999 Arp2/3 complex and actin depolymerization factor/cofilin in dendritic organization and treadmilling of actin filament array in Lamellipodia *J. Cell. Biol.* **145** 1009–26
- [9] Reymann A-C et al 2010 Nucleation geometry governs ordered actin networks structures *Nat. Mater.* **9** 827–32
- [10] Lieleg O et al 2009 Structural polymorphism in heterogeneous cytoskeletal networks *Soft Matter* **5** 1796–803
- [11] Borukhov I, Bruinsma R F, Gelbart W M and Liu A J 2005 Structural polymorphism of the cytoskeleton: a model of linker-assisted filament aggregation *PNAS* **102** 3673–8
- [12] Lee K-C, Borukhov I, Gelbart W M, Liu A J and Stevens M J 2004 Effect of mono- and multivalent salts on angle-dependent attractions between charged rods *Phys. Rev. Lett.* **93** 128101
- [13] Schmoller K M, Lieleg O and Bausch A R 2008 Cross-linking molecules modify composite actin networks independently *Phys. Rev. Lett.* **101** 118102
- [14] Kayser J, Grabmayr H, Harasim M, Herrmann H and Bausch A R 2012 Assembly kinetics determine the structure of keratin networks *Soft Matter* **8** 8873–9
- [15] Falzone T T, Lenz M, Kovar D and Gardel M L 2012 Assembly kinetics determine the architecture of α -actinin crosslinked F-actin networks *Nat. Commun.* **3** 861
- [16] Falzone Tobias T, Oakes Patrick W, Sees J, Kovar D and Gardel Margaret L 2013 Actin assembly factors regulate the gelation kinetics and architecture of F-actin networks *Biophys. J.* **104** 1709–19
- [17] Alvarado J, Mulder B M and Koenderink G H 2014 Alignment of nematic and bundled semiflexible polymers in cell-sized confinement *Soft Matter* **10** 2354–64
- [18] Soares e Silva M et al 2011 Self-organized patterns of actin filaments in cell-sized confinement *Soft Matter* **7** 10631–41
- [19] Limozin L and Sackmann E 2002 Polymorphism of cross-linked actin networks in giant vesicles *Phys. Rev. Lett.* **89** 168103
- [20] Deshpande S and Pfohl T 2012 Hierarchical self-assembly of actin in micro-confinements using microfluidics *Biomicrofluidics* **6** 0341201
- [21] Liu A P et al 2008 Membrane-induced bundling of actin filaments *Nat. Phys.* **4** 789–93
- [22] Tang J X and Janmey P A 1996 The polyelectrolyte nature of F-actin and the mechanism of actin bundle formation *J. Biol. Chem.* **271** 8556–63
- [23] Hosek M and Tang J X 2004 Polymer-induced bundling of F actin and the depletion force *Phys. Rev. E* **69** 051907
- [24] Ellis R J 2001 Macromolecular crowding: obvious but underappreciated *Trends Biochem. Sci.* **26** 597–604
- [25] Huber F, Strehle D and Käs J 2012 Counterion-induced formation of regular actin bundle networks *Soft Matter* **8** 931–6
- [26] Zhou H X, Rivas G N and Minton A P 2008 Macromolecular crowding and confinement: biochemical, biophysical, and potential physiological consequences *Ann. Rev. Biophys.* **37** 375–97
- [27] Kobayashi K, Huang C-I and Lodge T P 1999 Thermoreversible gelation of aqueous methylcellulose solutions *Macromolecules* **32** 7070–7
- [28] Köhler S, Lieleg O and Bausch A R 2008 Rheological characterization of the bundling transition in F-actin solutions induced by methylcellulose *PLoS ONE* **3** e2736
- [29] Tharmann R, MMAE C and Bausch A R 2006 Micro- and macrorheological properties of actin networks effectively cross-linked by depletion forces *Biophys. J.* **90** 2622–7
- [30] Nguyen L T, Yang W, Wang Q and Hirst L S 2009 Molecular dynamics simulation of F-actin reveals the role of cross-linkers in semi-flexible filament assembly *Soft Matter* **5** 2033–6
- [31] Doi M and Edwards S F 1999 *The Theory of Polymer Dynamics* (Oxford: Clarendon)
- [32] Narayanan J, Xiong J-Y and Liu X-Y 2006 Determination of agarose gel pore size: absorbance measurements vis a vis other techniques *J. Phys.: Conf. Series* **28** 83
- [33] Surrey T, Nédélec F, Leibler S and Karsenti E 2001 Physical properties determining self-organization of motors and microtubules *Science* **292** 1167–71
- [34] Nedelec F J, Surrey T, Maggs ac and Leibler S 1997 Self-organization of microtubules and motors *Nature* **389** 305–8
- [35] Backouche F, Haviv L, Groswasser D and Bernheim-Groswasser A 2006 Active gels: dynamics of patterning and self-organization *Phys. Biol.* **3** 264–73
- [36] Smith D et al 2007 Molecular motor-induced instabilities and cross linkers determine biopolymer organization *Biophys. J.* **93** 4445–52
- [37] Angelini T E, Liang H, Wriggers W and Wong G C L 2005 Direct observation of counterion organization in F-actin polyelectrolyte bundles *Eur. Phys. J. E* **16** 389–400
- [38] Gentry B, Smith D and Käs J A 2009 Buckling-induced zebra stripe patterns in nematic F-actin *Phys. Rev. E* **79** 031916
- [39] Bausch A R and Kroy K 2006 A bottom-up approach to cell mechanics *Nat. Phys.* **2** 231
- [40] Hall D and Minton A P 2003 Macromolecular crowding: qualitative and semiquantitative successes, quantitative challenges *BBA Proteins and Proteomics* **1649** 127–39
- [41] Madden T L and Herzfeld J 1993 Crowding-induced organization of cytoskeletal elements: I. Spontaneous demixing of cytosolic proteins and model filaments to form filament bundles *Biophys. J.* **65** 1147–54
- [42] Isambert H et al 1995 Flexibility of actin filaments derived from thermal fluctuations *J. Biol. Chem.* **270** 11437–44
- [43] Rezakhanliha R et al 2012 Experimental investigation of collagen waviness and orientation in the arterial adventitia using confocal laser scanning microscopy *Biomech. Model Mechanobiol.* **11** 461–73